NJC

Accepted Manuscript

This is an *Accepted Manuscript*, which has been through the Royal Society of Chemistry peer review process and has been accepted for publication.

Accepted Manuscripts are published online shortly after acceptance, before technical editing, formatting and proof reading. Using this free service, authors can make their results available to the community, in citable form, before we publish the edited article. We will replace this *Accepted Manuscript* with the edited and formatted *Advance Article* as soon as it is available.

You can find more information about *Accepted Manuscripts* in the Information for Authors.

Please note that technical editing may introduce minor changes to the text and/or graphics, which may alter content. The journal's standard Terms & Conditions and the Ethical guidelines still apply. In no event shall the Royal Society of Chemistry be held responsible for any errors or omissions in this *Accepted Manuscript* or any consequences arising from the use of any information it contains.

ROYAL SOCIETY OF CHEMISTRY

www.rsc.org/njc

New Journal of Chemistry

ARTICLE

Highly Productive Cobalt Nanoparticles Supported on Mesocellular Silica Foam for Fischer-Tropsch Reaction

Received 00th January 20xx,
Accepted 00th January 20xx

DOI: 10.1039/x0xx00000x

www.rsc.org/

Ji Chan Park,*[a,b] Jae In Kwon,[a] Shin Wook Kang,[a] Dong Hyun Chun,[a,b] Heon Jung,[a] Ho-Tae Lee,[a] Jung-Il Yang*[a]

We prepared highly productive Co/MCF nanocatalysts by a facile melt infiltration process using a hydrated Co precursor. The highly loaded Co particles (30 wt%) were uniformly dispersed in the large pores (30 nm) of the MCF support. The Co particles had an average diameter of 17 nm and clean surfaces without any surfactant. The Co/MCF catalyst exhibited very high hydrocarbon productivity (~0.98 $g_{total\ HC}\cdot g_{cat}^{-1}\cdot h^{-1}$) with high activity (CO conversion= 77%, CTY = 7.6 x 10^{-5} $mol_{CO}\cdot g_{Co}^{-1}\cdot s^{-1}$), and good selectivity for C_{5+} long chain hydrocarbons (~81%) in Fischer-Tropsch synthesis.

Introduction

Fischer-Tropsch synthesis (FTS) has been a key technology for producing clean alternative fuels from coal, natural gas, and biomass-derived syngas (CO and H_2).[1-5] With FTS, high molecular weight hydrocarbons (waxes) can be effectively produced using a Co-based catalyst, which has higher FTS activity, selectivity to linear paraffins, and lower water-gas-shift (WGS) activity than those of a Fe-based catalyst.[6-7] In general, such catalysts have been typically prepared by impregnation, co-precipitation, sol-gel, colloid, and micro-emulsion methods.[8] The catalytic behaviour is largely dependent on the nature of the Co species, particle size and dispersion, and support texture.[9-12] Until now, gamma-alumina (γ-Al_2O_3), a support that strongly interacts with active Co particles, has been used in order to minimize particle sintering by retarding crystallite diffusion.[13-14] Furthermore, small amounts of noble metals such as Pt and Ru have been used as promoters to enhance the reducibility of Co_3O_4 crystallites, and Co particle dispersion after reduction. This has resulted in a significant increase in the FT reaction rate.[15-16] However, conventional alumina supports have relatively small pore volumes (0.4–0.6 $cm^3\cdot g^{-1}$), low surface areas (200–300 $m^2\cdot g^{-1}$) and porosity, compared to those of mesoporous silica supports.[17-18] As a consequence, the active cobalt loading in alumina-based catalysts has generally been fixed at about 15 wt% in total catalyst weight, in order to prevent catalyst deactivation, which is caused by severe particle agglomeration during FTS.[19]

In the past few decades, mesoporous structures with well-defined pores (2–50 nm) and high surface areas have attracted interest as nanoparticle supporters, based on their textural properties, pore-size distribution, and acid/base characteristics.[20] In particular, ordered mesoporous silica (OMS) materials (e.g. MCM-41, KIT-6, and SBA-15), which are normally prepared using oil-in-water micro-emulsion templates, have received increasing attention as supports for catalysis due to their high thermal stability and easily controllable multi-function surfaces.[21-23] Among the various silica supports, siliceous mesostructured cellular foams (MCFs) have exhibited well-defined spherical cells (20–40 nm) and very large pore volumes (1.4–2.4 $cm^3\cdot g^{-1}$) as well as high surface areas (550–1000 $m^2\cdot g^{-1}$).[24]

Recently, de Jong et al. reported Co_3O_4/SiO_2 catalysts with small Co_3O_4 crystallite sizes ranging from 4–10 nm, fabricated by an easy and fast melt infiltration process.[25] However, the load of active Co metals was still restricted to the range of 10–22 wt%, in order to maintain the particle dispersion. This was due to the limited pore volumes (<1.0 $cm^3\cdot g^{-1}$) and pore sizes (~9 nm) of the silica supports used.

Recently, highly metal-loaded catalysts (above 20 wt%) were developed, with uniform particle dispersion on a carbon support which had large pore volume and porosity, and demonstrated increased productivity for Suzuki-Miyaura coupling reactions, compare to that of a commercial catalyst.[26] In the same way, the use of higher Co loaded catalyst in FTS could lead to an increased number of Co sites if the particle dispersion can be maintained. This should result in high production of valuable liquid oil and solid wax.

Herein, we report a Co/MCF nanocatalyst for FTS, which contains active and well-dispersed Co nanoparticles (17 nm) with very high loading (30 wt%). It was created via melt

[a]Clean Fuel Laboratory, Korea Institute of Energy Research, 152 Gajeong-Ro, Daejeon, 305-343, Korea. E-mail: jcpark@kier.re.kr; yangji@kier.re.kr; Tel:+82-42-860-3605
[b]Advanced Energy and Technology, University of Science and Technology, 217 Gajeong-Ro, Daejeon, 305-350, Korea

† Footnotes relating to the title and/or authors should appear here.
Electronic Supplementary Information (ESI) available: [details of any supplementary information available should be included here]. See DOI: 10.1039/x0xx00000x

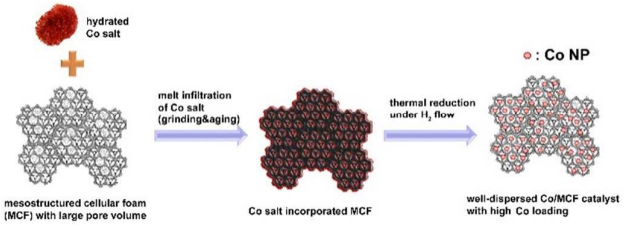

Scheme 1. Scheme for synthesis of the Co/MCF nanocatalyst

infiltration of a hydrated Co salt into silica pores and subsequent thermal reduction of the salt inside (**Scheme 1**).

Experimental

Chemicals. Cobalt(II) nitrate hexahydrate ($Co(NO_3)_2 \cdot 6H_2O$, ≥98%), tetraethyl orthosilicate (TEOS, 98%), mesitylene (98%), and ammonium fluoride (NH_4F, ≥98%), were purchased from Aldrich. Ammonium hydroxide (NH_4OH, 28% in water) and hydrochloric acid (HCl, 35% in water) were obtained from Junsei. Gamma-alumina powder (Al_2O_3, ≥97%) was purchased from Strem Chemicals, Inc. All chemicals were used as received without further purification.

Preparation of MCF. The mesostructured cellular foam (MCF) was prepared using a hydrothermal method. First, Pluronic P123 (8.0 g) was completely dissolved in hydrochloric acid (1.6 M, 300 mL) at room temperature. Mesitylene (14.2 mL) and NH_4F (92 mg) were added, and the mixture was heated to 333 K and stirred for 1 h. After that, TEOS (19.2 mL) was added to the mixture solution and was stirred for 20 h at the same temperature. After 20 h, the resulting slurry was aged in an oven at 373 K for 24 h. The suspension was precipitated by centrifugation, washed with water and ethanol thoroughly, and dried for 48 h under ambient conditions. The final white product was calcined in a box-type furnace at 873 K for 12 h.

Preparation of Co/MCF and Co/Al_2O_3. For synthesis of the Co/MCF catalyst, $Co(NO_3)_2 \cdot 6H_2O$ (2.1 g) and MCF powder (1.0 g) were physically ground in a mortar for several minutes. After grinding under ambient conditions, the resulting pink powder was aged at 333 K for 24 h. After aging, the sample was cooled to room temperature and transferred to an alumina boat in a tube-type furnace. Finally, the cobalt-incorporated powder was slowly heated at a ramping rate of 4 $K \cdot min^{-1}$ up to 773 K under a continuous H_2 flow of 0.2 $L \cdot min^{-1}$ and calcined at 773 K for 4 h. After calcination, the resulting powder was cooled down to room temperature and immediately submerged in ethanol (20 mL) under a vigorous N_2 flow of 1.0 $L \cdot min^{-1}$ in order to minimize surface oxidation of the cobalt particles. The Co/MCF powder immersed in ethanol was separated by magnet and dried in a vacuum oven at 333 K. The procedure for preparation of Co/Al_2O_3 was identical to the procedure for preparing Co/MCF, except for the use of gamma-alumina powder (1.0 g) as a support material.

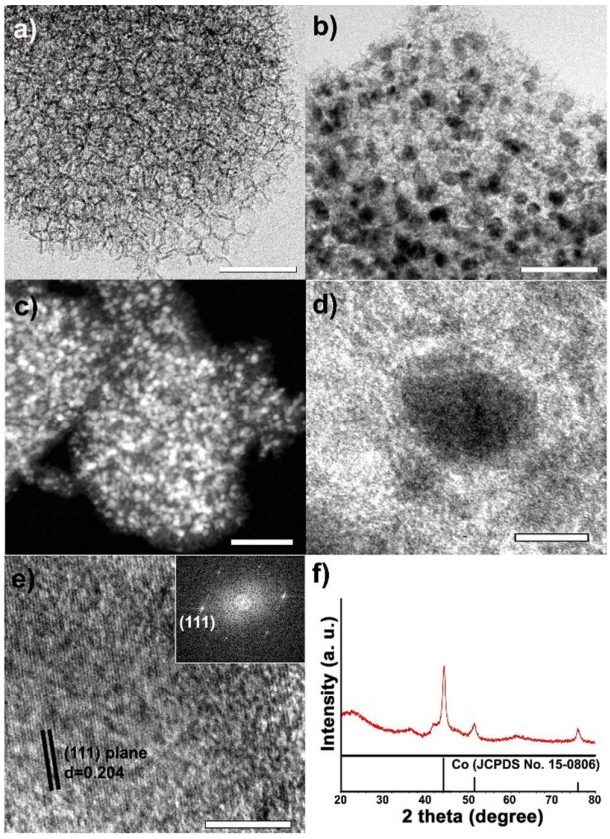

Fig. 1 TEM images of (a) bare MCF support and (b-d) Co/MCF nanocatalyst. (e) HRTEM image with the corresponding FT pattern (inset of e) and (f) XRD spectrum of Co/MCF nanocatalyst. The bars indicate 100 nm (a–b), 200 nm (c), 10 nm (d), and 5 nm (e).

Fischer-Tropsch synthesis. Fischer-Tropsch (FT) reactions were performed in a down-flow fixed-bed stainless steel reactor tube with an inner diameter of 5 mm and 180 mm length. Typically, the catalyst (0.5 g) was diluted with glass beads (425-600 μm, 2.5 g) to prevent hot-spot generation, and then loaded in the catalyst bed. Before reaction, the catalysts were reduced in situ at atmospheric pressure by passing a flow of H_2 (80 $mL \cdot min^{-1}$) at 673 K for 2 h. After reduction, the reaction was carried out at 503 K and 20 bar for 36 h using a reactant gas (H_2/CO = 2.0, GHSV = 6.8 $NL \cdot g_{cat}^{-1} \cdot h^{-1}$). The composition of the outlet gases was analysed using a gas chromatograph (DS Science, iGC7200) equipped with a thermal conductivity detector (TCD) and a flame ionization detector (FID). The flow rates of the outlet gases were measured using a wet-gas flow meter (Shinagawa Co.). After FT reaction for 36 h, the solid hydrocarbon products were collected in a hot trap (513 K) and the liquid hydrocarbon products and water were collected in a cold trap (273 K). The isolated wax and liquid products were

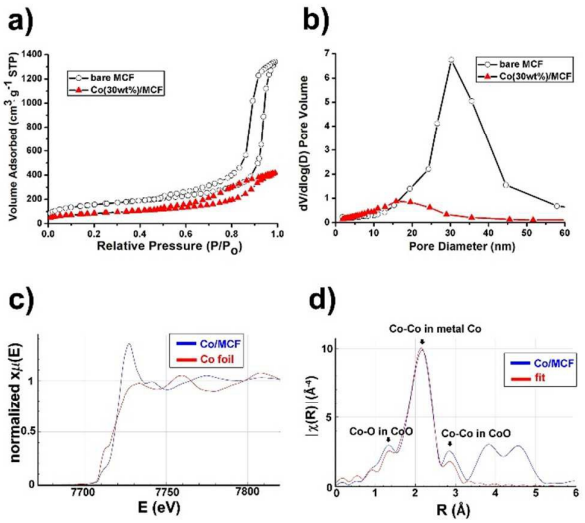

Fig. 2 (a) N_2 adsorption/desorption isotherms, (b) pore size distribution diagrams, (c) XANES and (d) EXAFS spectra of the Co/MCF nanocatalyst.

analysed using an offline gas chromatograph (Agilent, 6890 N) and the simulated distillation method (ASTM D2887). CO conversion and hydrocarbon product selectivity were calculated using an equation from the literature.[27]

Characterization. The catalysts were characterized using transmission electron microscopy (Tecnai G2 F30 operated at 300 kV, KAIST) and high power powder-XRD (Rigaku D/MAX-2500, 18 kW). For TEM analysis, samples were prepared by putting a few drops of the corresponding colloidal solutions on Formvar carbon-coated copper grids (Ted Pellar, Inc). Nitrogen sorption isotherms were measured at 77 K with a Tristar II 3020 surface area analyser. Before measurements, the samples were degassed in a vacuum at 573 K for 4 h. The Co X-ray absorption spectra (XAS) were recorded on Beam-line 6D of the Pohang Accelerator Laboratory (PAL).

Results and discussion

Synthesis of Co/MCF catalyst

Scheme 1 demonstrates the overall synthetic procedure for the Co/MCF catalyst. First, the MCF, which has a well-defined ultra large mesoporous and hydrothermally robust framework, was synthesized using a hydrothermal method according to the literature.[28] Pluronic P123 triblock copolymer was used as a structure directing agent.

The transmission electron microscopy (TEM) image of the MCF indicates cells constructed of silica struts (**Fig. 1a**). The large cells (~30 nm) were connected by windows (~18 nm). Next, the active Co nanoparticles were simply embedded in the MCF support by the melt infiltration method using hydrated Co salt.[25] To prepare a 30 wt% cobalt-loaded Co/support catalyst, the $g_{Co\ salt}/g_{support}$ ratio of 2.1 was used.

Based on the complete infiltration of the salt into the large pores of the MCF, small Co nanoparticles were regularly formed after thermal decomposition and reduction. The TEM image shows incorporated Co nanoparticles with an average diameter of 17.4±2.0 nm (**Fig. 1b**). The high-angle annular dark-field scanning transmission electron microscopy (HAADF-STEM) image indicates relatively bright spots that originate from the heavier Co atoms (than Si) (**Fig. 1c**). High-resolution TEM (HRTEM) analysis also revealed a single Co nanoparticle in a silica cell (**Fig. 1d**). The HRTEM image and the corresponding Fourier-Transform (FT) pattern show the single crystalline nature of the Co particles (**Fig. 1e**). The lattice distance of 0.204 nm between the neighbouring fringes corresponded to the lattice spacing of Co (111) (**inset of Fig. 1e**). The X-ray diffraction (XRD) spectrum of Co/MCF has a sharp peak at 2θ = 44°, which is assigned to the reflections of the (111) plane in the fcc-Co phase (**Fig. 1f**, JCPDS No. 15-0806). The average size of the Co crystals was estimated to be 16.7 nm, from the broadness of the (111) peak by the Debye-Scherrer equation, which well-matched that observed in the TEM images.

The N_2 sorption experiment at 77 K for the Co/MCF catalyst exhibited type IV adsorption-desorption hysteresis (**Fig. 2a**). The Brunauer-Emmett-Teller (BET) surface areas of the bare MCF and the Co/MCF were calculated to be 560.7 $m^2 \cdot g^{-1}$ and 289.0 $m^2 \cdot g^{-1}$, respectively. The total pore volume of the Co/MCF catalyst (0.65 $cm^3 \cdot g^{-1}$) was much lower than that of the bare MCF support (2.07 $cm^3 \cdot g^{-1}$) because of the highly loaded Co in the silica. The pore size of the Co/MCF catalyst was found to be 16 nm, using the Barrett-Joyner-Halenda (BJH) method on the adsorption branch (**Fig. 2b**). The observed pore size was dramatically decreased from 30 nm in bare MCF to 16 nm in Co/MCF, reflecting the pore volume filled by Co nanoparticles. The Co-loading content for the Co/MCF catalyst was calculated to be nominally 30 wt% on the basis of Co converted from the cobalt nitrate salt after thermal treatment.

X-ray absorption spectroscopy (XAS) provided valuable information about the oxidation state and structure of the cobalt catalyst. The XAS measurement of Co/MCF was conducted at the K edge of cobalt (7709 eV). In the X-ray absorption near-edge structure (XANES) region from one absorption edge to 7759 eV, a Co pre-edge peak of the Co/MCF catalyst was observed both at 7709 and 7718 eV, which match the peaks of Co and CoO, respectively (**Fig. 2c**). The extended X-ray absorption fine structure (EXAFS) pattern of the Co/MCF catalyst also shows the three major peaks of the first coordination shells of Co and CoO structures, originating from Co–O in CoO, Co-Co in Co, and Co-Co in CoO scattering (**Fig. 2d**). Even though the fresh Co/MCF catalyst powder was directly passivated by ethanol after reduction, partial surface oxidation was inevitable during catalyst analysis under ambient conditions. This was because the metallic Co nanoparticles in the silica pores are highly sensitive to oxygen exposure.

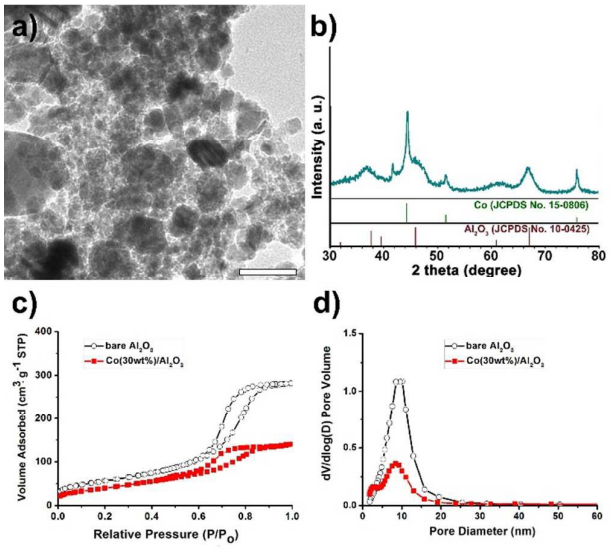

Fig. 3 (a) TEM image, (b) XRD spectrum, (c) N_2 adsorption/desorption isotherms, and (d) pore size distribution diagrams of Co/Al_2O_3 catalyst. The bar in (a) indicates 50 nm.

Synthesis of Co/Al_2O_3 catalyst

The preparation of gamma(γ)-alumina-supported Co nanoparticles (Co/Al_2O_3) was conducted identically to the procedure for Co/MCF, except for the use of alumina powder instead of MCF. Highly irregular Co particles that ranged from about 2–50 nm were observed in the TEM image, compared to those of Co/MCF (**Fig. 3a**). The large Co nanoparticles on the alumina support were generated because the pore volume of the alumina is insufficient for filling with a large amount of molten Co salts. The XRD spectrum also shows a sharp peak at $2\theta = 44°$, reflecting a larger Co-crystal size. This was calculated to be 24.7 nm, based on the (111) peak (**Fig. 3b**). Alumina peaks were mainly observed at $2\theta = 37.6°$, 45.9°, and 67.0°; corresponding to the reflections of the (311), (400), and (440) planes, respectively.

N_2 sorption experiments at 77 K for bare alumina and Co/Al_2O_3 catalyst exhibited type IV adsorption-desorption hysteresis (**Fig. 3c**). The BET surface areas of bare Al_2O_3 and Co/Al_2O_3 were calculated to be 205.0 $m^2 \cdot g^{-1}$ and 144.7 $m^2 \cdot g^{-1}$, respectively. The total pore volumes were 0.44 $cm^3 \cdot g^{-1}$ in the initial AlO_3 support and 0.22 $cm^3 \cdot g^{-1}$ in Co/Al_2O_3. The pore size of the Al_2O_3 support was found to be 10.1 nm, using the BJH method on the adsorption branch (**Fig. 3d**). In the Co/Al_2O_3 catalyst, slightly reduced pore size (8.4 nm) was observed because of Co nanoparticles that filled the alumina pores.

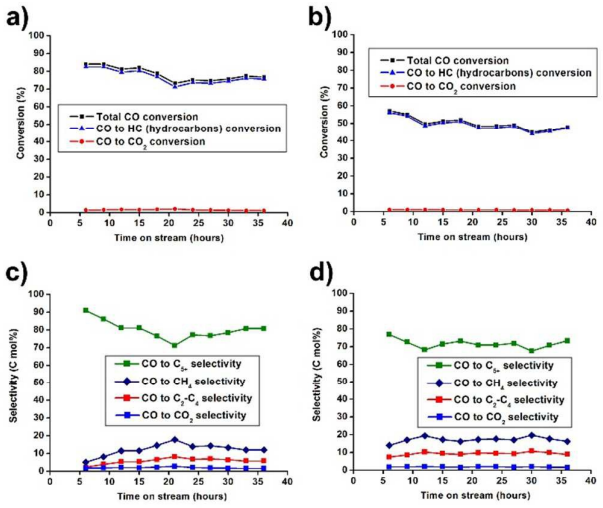

Fig. 4 CO conversion and hydrocarbon product selectivity graphs of (a,c) Co/MCF and (b,d) Co/Al_2O_3 catalysts. The total CO conversion is the sum of the CO conversion to hydrocarbons (CO to HC) and the CO conversion to CO_2 (CO to CO_2).

Reactivity and productivity comparison between Co/MCF and Co/Al_2O_3 in the Fischer–Tropsch synthesis reaction

Fischer-Tropsch (FT) reaction tests were carried out at 20 bar, 230 °C, and an H_2/CO ratio of '2', using the Co/MCF and Co/Al_2O_3 catalysts. The CO conversion and selectivity of the catalysts were measured for 36 h over time-on-stream (TOS) of a reaction by gas chromatography (GC) analysis of the outlet gases containing the unreacted CO, H_2, CH_4, C_2-C_4 hydrocarbons, and CO_2. Liquid hydrocarbons obtained in a cold trap and solid hydrocarbons obtained in a hot trap were analysed by simulated distillation (SIMDIS). The hydrocarbon formation proceeds by FTS as follows:

$$nCO + (2n+1)H_2 \rightarrow C_nH_{2n+2} + nH_2O : \text{FTS (paraffins)}$$

$$nCO + 2nH_2 \rightarrow C_nH_{2n} + nH_2O : \text{FTS (olefins)}$$

$$CO + H_2O \leftrightarrow CO_2 + H_2 : \text{WGS}$$

The Co/MCF catalyst quickly reached a steady-state within 6 h of reaction and showed much higher total CO conversion (76.8%) than that of Co/Al_2O_3 (47.9%) at TOS 36 h (**Fig. 4a-b**). Furthermore, in the selectivity data, the graph of Co/MCF shows a high C_{5+} (80.8%) at TOS 36 h with low selectivity of CO_2 (1.5%), CH_4 (12.0%), and C_2–C_4 (5.7%) (**Fig. 4c**). On the other hand, for Co/Al_2O_3, higher selectivity of CH_4 (16.2%) and C_2–C_4 (8.8%), and lower selectivity of C_{5+} (73.3%) were obtained (**Fig. 4d**).

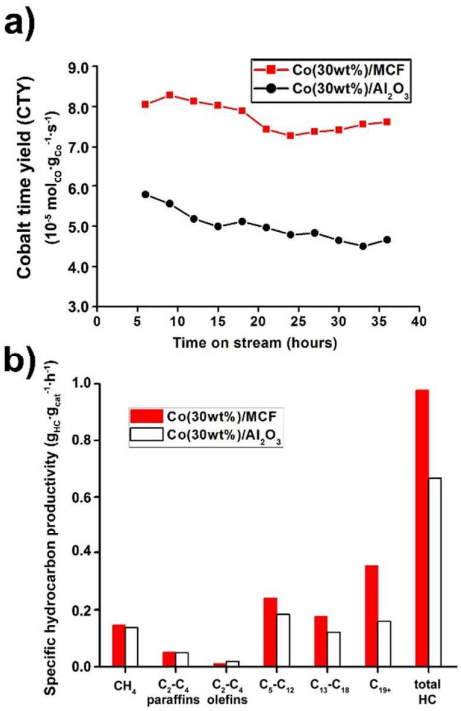

Fig. 5 (a) Cobalt time yield and (b) hydrocarbon productivity data of the Co/MCF and Co/Al_2O_3 catalysts.

CH_4 selectivity was dependent on cobalt particle size.[29] De Jong et al. reported that Co particles smaller than 6 nm show rather low activity because of blocking of edge/corner sites with a lower intrinsic activity at small terraces, as well as their high hydrogen coverages.[30-31] In addition, the small Co particles (1.4–2.5 nm) can be easily oxidized by the water vapour formed during the FT reaction, resulting in lower activity and higher CH_4 selectivity.[32] However, most of the Co nanoparticles in the MCF pores would be stable against surface oxidation during the FT reaction, based on their adequate and regular particle size (17 nm). On the other hand, in the Co/Al_2O_3 catalyst, which has a very broad particle size distribution, the small Co nanoparticles (< 3 nm) could be unstable to re-oxidation by water vapour during the FT reaction. Furthermore, the regular mesoporous pores can be beneficial, in terms of mass transfer of the reactants. In the case of the Co/Al_2O_3 catalyst, the big and irregular particles (> 30 nm) located on the pores could hinder reactant diffusion to small Al_2O_3 pores (10 nm). The diffusion limitations for CO in the catalyst pores could cause a higher H_2/CO ratio in the catalyst pores, resulting in methane formation. Therefore, the uniform Co/MCF catalyst showed lower methane selectivity and higher C_{5+} selectivity than those of the irregular Co/Al_2O_3 catalyst.

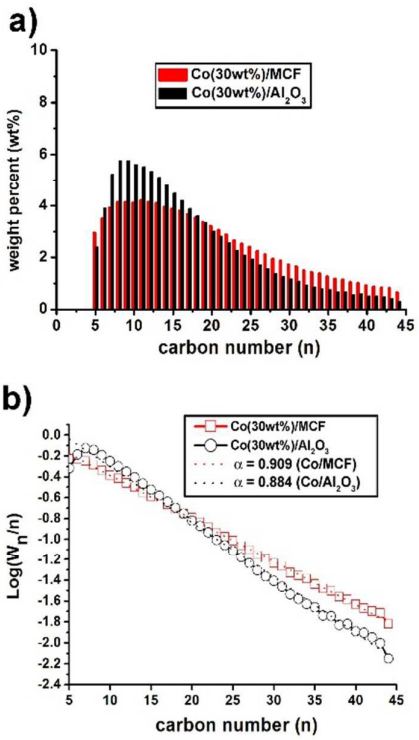

Fig. 6 (a) Hydrocarbon product distributions and (b) ASF plots of C_{5+} hydrocarbons and carbon chain growth probability.

The FT activity was noted to be the cobalt time yield (CTY, the number of CO moles converted to hydrocarbons per gram of cobalt per second) over time-on-stream (TOS) (**Fig. 5a**). For the Co/MCF catalyst, the CTY at 36 h was 7.6×10^{-5} $mol_{CO} \cdot g_{Co}^{-1} \cdot s^{-1}$, which is much higher than that (4.7×10^{-5} $mol_{CO} \cdot g_{Co}^{-1} \cdot s^{-1}$) of Co/Al_2O_3. The site time yield (STY) values were calculated to be 10.8 x $10^{-2} \cdot s^{-1}$ for Co/MCF and 7.4 x $10^{-2} \cdot s^{-1}$ for Co/Al_2O_3, respectively, based on the Co dispersion (0.0414: Co/MCF, 0.0373: Co/Al_2O_3) obtained by H_2 chemisorption.

The high FT activity of the Co/MCF catalyst is attributed to its having more Co active sites with higher activity, based on its higher particle dispersion with the smaller Co particle size than Co/Al_2O_3, even with its high Co loading amount of 30 wt%. This high FT activity in Co/MCF is comparable to the previously reported values in various Co nanocatalysts. In previous works, Co/SiO_2 and Co/C supported catalysts showed relatively low FT activities of 3.0–6.0 × 10^{-5} $mol_{CO} \cdot g_{Co}^{-1} \cdot s^{-1}$.[33-35]

Table 1. Hydrocarbon product distributions (wt%)

Product / Catalyst	CH_4	C_2-C_4	C_5-C_{12}	C_{13}-C_{18}	C_{19+}
Co/MCF	14.9	6.3	24.5	18.1	36.2
Co/Al_2O_3	20.6	10.0	27.5	18.1	23.8

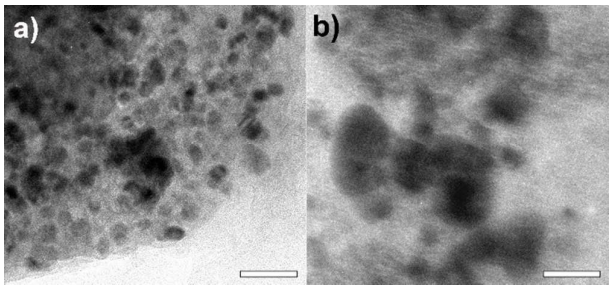

Fig. 7 TEM images of the recovered (a) Co/MCF and (b) Co/Al_2O_3 catalysts after the FT reaction. All bars indicate 50 nm.

The Co/MCF catalyst also showed very high C_{5+} productivity (0.77 $g_{C5+\ HC}{\cdot}g_{cat}^{-1}{\cdot}h^{-1}$), which is the sum of the liquid oil productivity (0.32 $g_{liq}{\cdot}g_{cat}^{-1}{\cdot}h^{-1}$) and solid wax productivity (0.45 $g_{sol}{\cdot}g_{cat}^{-1}{\cdot}h^{-1}$). On the other hand, the Co/Al_2O_3 catalyst showed lower C_{5+} productivity (0.46 $g_{C5+\ HC}{\cdot}g_{cat}^{-1}{\cdot}h^{-1}$), based on its poor liquid oil productivity (0.22 $g_{liq}{\cdot}g_{cat}^{-1}{\cdot}h^{-1}$) and solid wax productivity (0.24 $g_{sol}{\cdot}g_{cat}^{-1}{\cdot}h^{-1}$). For the Co/MCF catalyst, the total hydrocarbon (HC) productivity from C_1 to C_{44} was measured to be 0.98 $g_{total\ HC}{\cdot}g_{cat}^{-1}{\cdot}h^{-1}$, which is 1.46 times higher than the 0.67 $g_{HC}{\cdot}g_{cat}^{-1}{\cdot}h^{-1}$ of Co/Al_2O_3 (**Fig. 5b**). In particular, the catalyst showed high productivity in the valuable solid- and liquid-products of the gasoline-range C_5–C_{12} (0.24 $g_{HC}{\cdot}g_{cat}^{-1}{\cdot}h^{-1}$), diesel- range C_{13}–C_{18} (0.18 $g_{HC}{\cdot}g_{cat}^{-1}{\cdot}h^{-1}$), and wax-range C_{19+} (0.35 $g_{HC}{\cdot}g_{cat}^{-1}{\cdot}h^{-1}$). The detailed composition of the liquid and solid hydrocarbons by ASTM D2887, and the total distributions of hydrocarbons including gaseous products were analysed (**Fig 6a, Table 1**). In total weight portions of CH_4, C_2–C_4, C_5–C_{12}, C_{13}–C_{18}, and C_{19+} of the catalysts, the heavy hydrocarbon portion (C_{19+}) was significantly high (36.2%) with Co/MCF.

Using the Anderson-Schulz-Flory (ASF) chain growth mechanism in the following equation,[36] the chain growth probability (a) of the hydrocarbons was calculated (**Fig. 6b**).

$$\log(W_n/n) = \log(\ln^2\alpha) + n\log\alpha$$

The α values were obtained from the slope of the graph from C_5 to C_{44}. The high α value (0.909) for Co/MCF demonstrates that the adequate and regular cobalt surface can provide more advantageous conditions for the growth of carbon chains during FT synthesis. However, in Co/Al_2O_3, a low α value (0.884) was observed. This was because of the presence of irregular and smaller Co nanoparticles (<10 nm) which have a high methane formation property. Low chain growth probability was found with high methane selectivity, resulting in lower selectivity to heavy weight hydrocarbons, as with Co/Al_2O_3. After the reactions, the Co/MCF catalyst maintained its original structures without severe particle aggregation, supported by well-organized silica frameworks containing Co particles (**Fig. 7a**). In contrast, a great deal of Co component with inhomogeneous particles on top of the support were observed in the Co/Al_2O_3 catalyst (**Fig. 7b**).

Conclusions

Mesocellular silica foam (MCF) is a good support which enables the high loading of active cobalt nanoparticles with uniform dispersion, because of its high porosity. A Co/MCF catalyst with high Co loading (30wt%) was prepared by a facile melt infiltration process, and showed high FT activity (7.6×10^{-5} $mol_{CO}{\cdot}g_{Co}^{-1}{\cdot}s^{-1}$). This was because of the well-dispersed and stable Co crystallite size (17 nm) in the uniform pores of the support. On the other hand, the Co/Al_2O_3 catalyst, with the same Co loading, exhibited much less catalytic performance under the same reaction conditions. This was due to its irregular particles which consisted of less active particles > 30 nm which blocked pores on the alumina support, and easily oxidizable particles (< 5nm) in the alumina pores. We have confirmed that the Co/MCF catalyst, with proper Co loading and using the highly porous MCF support, exhibits very significant hydrocarbon productivity based on its relatively higher number of active sites and its high activity and selectivity for C_{5+} long-chain hydrocarbons during Fischer-Tropsch synthesis.

Acknowledgements

This research was supported by the Research and Development Program of the Korea Institute of Energy Research (KIER) (B6-2439).

Notes and references

1 H. Schulz, *Appl. Catal. A: Gen.,* 1999, **186**, 3.
2 M. E. Dry, *Catal. Today*, 2002, **71**, 227.
3 A. de Klerk, *Green Chem.,* 2008, **10**, 1249.
4 E. van Steen and M. Claeys, *Chem. Eng. Technol.*, *2008*, **31**, 655.
5 O. O. James, B. Chowdhury, M. A. Mesubi and S. Maity, *RSC Adv.*, 2012, **2**, 7347.
6 Q. Zhang, J. Kang and Y. Wang, *ChemCatChem,* 2010, **2**, 1030.
7 S. K. Beaumont, *Phys. Chem. Chem. Phys.*, 2014, **16**, 5034.
8 A. Y. Khodakov, W. Chu and P. Fongarland, *Chem. Rev.*, 2007, **107**, 1692.
9 D. J. Kim, B. C. Dunn, P. Cole, G. Turpin, R. D. Ernst, R. J. Pugmire, M. Kang, J. M. Kim and E. E. Eyring, *Chem. Commun.*, 2005, 1462.
10 J. Zhang, J. Chen, J. Ren and Y. Sun, *Appl. Catal. A: Gen.*, 2003, **243**, 121.
11 A. Y. Khodakov, R. Bechara and A. Griboval-Constant, *Appl. Catal. A: Gen.*, 2003, **254**, 273.
12 I. T. Ghampson, C. Newman, L. Kong, E. Pier, K. D. Hurley, R. A. Pollock, B. R. Walsh, B. Goundie, J. Wright, M. C. Wheeler,

R. W. Meulenberg, W. J. DeSisto, B. G. Frederick and R. N. Austin, *Appl. Catal. A: Gen.*, 2010, **388**, 57.
13 J.-H. Oh., J. W. Bae, S.-J. Park, P. K. Khanna and K.-W. Jun, *Catal. Lett.*, 2009, **130**, 403.
14 Ø. Borg, S. Eri, E. A. Blekkan, S. Storsæter, H. Wigum, E. Rytter and A. Holmen, *J. Catal.,* 2007, **248**, 89.
15 W. Chu, P. A. Chernavskii, L. Gengembre, G. A. Pankina, P. Fongarland and A. Y. Khodakov, *J. Catal.*, 2007, **252**, 215.
16 C. Pirola, M. Scavini, F. Galli, S. Vitali, A. Comazzi, F. Manenti and P. Ghigna, *Fuel*, 2014, **132**, 62.
17 M. Trueba and S. P. Trasatti, *Eur. J. Inorg. Chem.*, 2005, 3393.
18 T. Klimova, P. M. Vara and I. P. Lee, *Catal. Today.*, 2010, **150**, 171.
19 W. Chu, L.-N. Wang, P. A. Chernavskii and A. Y. Khodakov, *Angew. Chem. Int. Ed.*, 2008, **47**, 5052.
20 A. Taguchi and F. Schüth, *Micropor. Mesopor. Mater.*, 2005, **77**, 1.
21 J. Panparnot, S. Kaewkun, P. Praserthdam and J. G. Goodwin, Jr., *Catal. Lett.*, 2003, **91**, 95.
22 M. K. Gnanmani, G. Jacobs, U. M. Graham, W. Ma, V. R. R. Pendyala, M. Ribeiro and B. H. Davis, *Catal. Lett.*, 2010, **134**, 37.
23 R. M. Rioux, H. Song, J. D. Hoefelmeyer, P. Yang and G. A. Somorjai, *J. Phys. Chem. B*, 2005, **109**, 2192.
24 Patrick Schmidt-Winkel, W. W. Lukens, Jr., P. Yang, D. I. Margolese, J. S. Lettow, J. Y. Ying and G. D. Stucky, *Chem. Mater.*, 2000, **12**, 686.
25 T. M. Eggenhuisen, J. P. den Breejen, D. Verdoes, P. E. de Jongh and K. P. de Jong, *J. Am. Chem. Soc.*, 2010, **132**, 18318.
26 H. Woo, K. Lee, J. C. Park and K. H. Park, *New J. Chem.,* 2014, **38**, 5626.
27 Y. Lu, P. Zhou, J. Han and F. Yu, *RSC Adv.*, 2015, **5**, 59792.
28 J. C. Park, J. U. Bang, J. Lee, C. H. Ko and H. Song, *J. Mater. Chem.*, 2010, **20**, 1239.
29 A. Barbier, A. Tuel, I. Arcon, A. Kodre and G. A. Martin, *J. Catal.,* 2010, **200**, 106.
30 J. P. den Breejen, P. B. Radstake, G. L. Bezemer, J. H. Bitter, V. Frøseth, A. Holmen and K. P. de Jong, *J. Am. Chem. Soc.*, 2009, **131**, 7197.
31 G. L. Bezemer, J. H. Bitter, H. P. C. E. Kuipers, H. Oosterbeek, J. E. Holewijn, X. Xu, F. Kapteijn, A. J. van Dillen and K. P. de Jong, *J. Am. Chem. Soc.*, 2006, **128**, 3956.
32 Z.-j. Wang, S. Skiles, F. Yang, Z. Yan and D. W. Goodman, *Catal. Today*, 2012, **181**, 75.
33 K.-S. Ha, G. Kwak, K.-W. Jun, J. Hwang and J. Lee, *Chem. Commun.*, 2013, **49**, 5141.
34 G. Kwak, J. Hwang, J.-Y. Cheon, M. H. Woo, K.-W. Jun, J. Lee and K.-S. Ha, *J. Phys. Chem. C*, 2013, **117**, 1773.
35 J. P. den Breejen, J. R.A. Sietsma, H. Friedrich, J. H. Bitter and K. P. de Jong, *J. Catal.*, 2010, **270**, 146.
36 R. S. Hurlbut, I. Puskas and D. J. Schumacher, *Energy Fuels*, 1996, 10, 537.

Graphical Abstract

The Co/MCF nanocatalyst containing well-dispersed and highly loaded Co nanoparticles exhibits very high hydrocarbon productivity in Fischer-Tropsch synthesis.